NUMERICAL STUDY OF THE EFFECTS OF BOUNDARY CONDITIONS ON THE MEASUREMENT AND CALIBRATION OF GARDON-TYPE HEAT FLUX SENSORS

M. Krane and A. Dybbs
Case Western Reserve University
Cleveland, Ohio

To monitor the high-intensity heat flux conditions that occur in the space shuttle main engine (SSME), it is necessary to use specifically designed heat flux sensors. These sensors, which are of the Gardon-type, are exposed on the measuring face to high-intensity radiative and convective heat fluxes and on the other face to convective cooling. To improve the calibration and measurement accuracy of these gauges, we are studying the effect that the thermal boundary conditions have on gauge performance. In particular, we are studying how convective cooling effects the field inside the sensor and the measured heat flux.

The first phase of this study involves a numerical study of these effects. Subsequent phases will involve experimental verification.

A computer model of the heat transfer around a Gardon-type heat flux sensor was developed. The results of this study will allow us to make corrections both in calibration and applications so that the input (hot-side) heat flux can be determined more accurately.

Two specific geometries are being considered as shown in figure 1:

(1) Heat flux sensor mounted on a flat-plate
(2) Heat flux sensor mounted at the stagnation point of a circular cylinder

Both of these configurations are representative of the use of heat flux sensors in the components of the SSME.

The purpose of the analysis is to obtain a temperature distribution as a function of the boundary conditions. Previous analyses of Gardon sensors have concentrated on the thin-foil part of the sensor, considering it to be attached to an infinite heat sink. This is a reasonable assumption at low temperatures, but at the high temperatures found in the SSME, this assumption is questionable. The results of this analysis will determine (1) how the cooling of a sensor in such extreme environments approximates the "thin-foil" assumption and (2) how nonuniformities in the cooling (caused by convection cooling coefficients being space dependent) effect the measurement of the hot-side heat flux.

The equations for the general case are shown in figure 2. We have not included in this formulation the thermal conductivity variations caused by the thermocouple wires or channels.

As a first test case, the following simplifications were made:

(1) Constant radiant hot-side heat flux
(2) Constant convection cooling coefficients and ambient temperatures
(3) Symmetrical k-distribution (i.e., no thermocouple wire or channels)
(4) Constant thermal conductivity

The first assumption eliminates natural convection or re-radiation cooling. We know how to handle both of these effects. The second and third assumptions eliminate any θ-dependence in the problem so that it is axisymmetric. Finally, the fourth assumption makes the problem a linear one.

A finite-difference model was used to solve the equations shown in figure 2. Several cases have been studied. The results are shown in figures 3 to 5. Figure 3 shows the calibration curves for a typical sensor. The top of the sensor has a convective heat-transfer coefficient $h_{top} = 10$ KW/m^2°K. This figure shows the results of varying the cooling or bottom side heat-transfer coefficient. For these cases, the sensitivity of the sensor decreases with an increase in the cooling heat-transfer coefficient. This result is also shown in figure 4 where the sensor sensitivity is plotted versus the cooling heat-transfer coefficient.

The cases studied in figures 3 and 4 were for radiation and convective heat fluxes at the top face of the sensors to be of the same order of magnitude. If the convective heat flux is small in comparison to the radiation heat flux, then the cooling heat transfer has little effect on the calibration curve. This is shown in figure 5 where the cases of figures 3 and 4 are compared to the case of $h_{top} = 0$ KW//m^2°K with varying cooling h's.

TWO GEOMETRIES:

1. FLAT PLATE

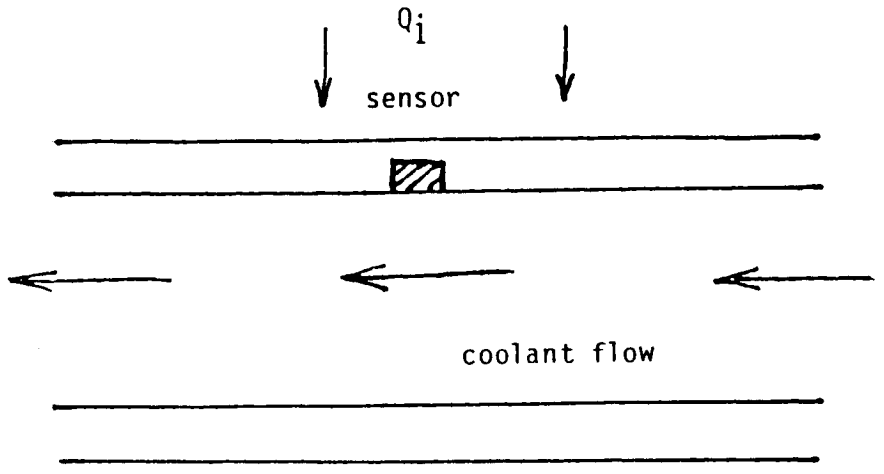

2. CYLINDER

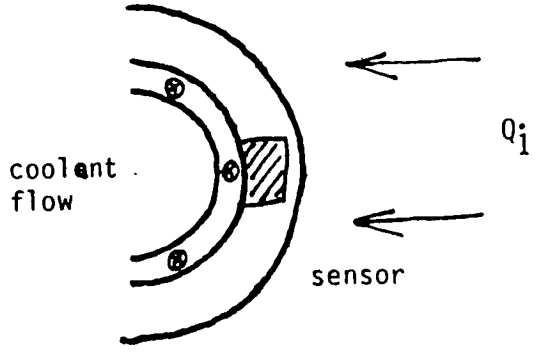

Figure 1. - Heat flux sensor configurations to be considered.

GENERAL CASE

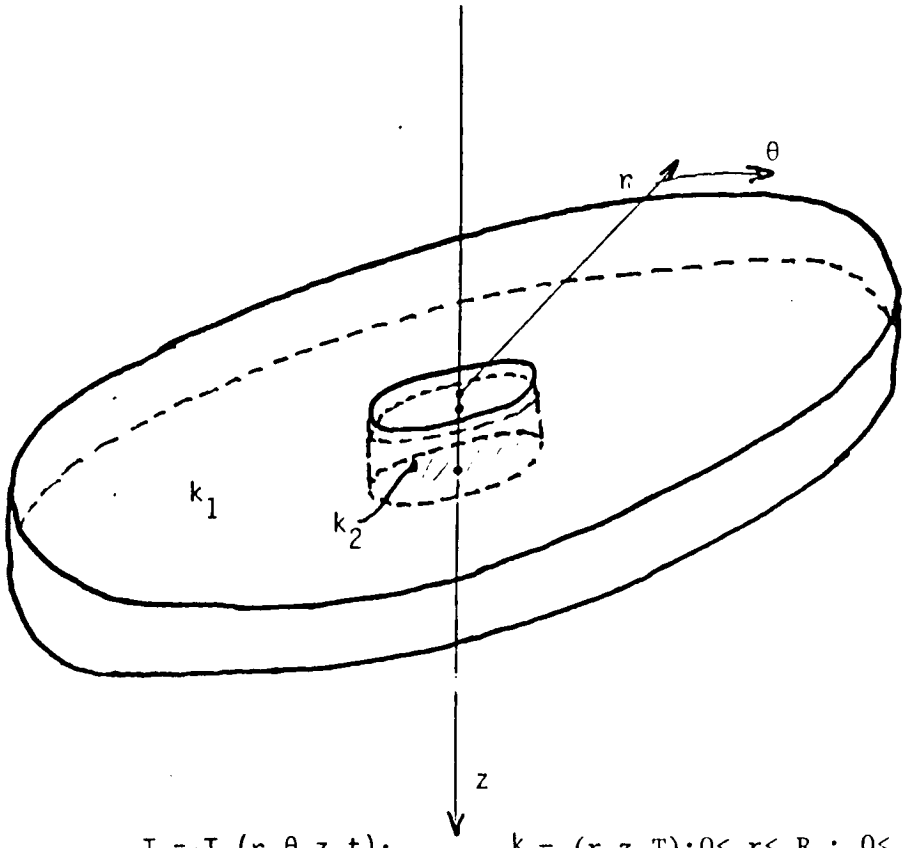

$$T = T(r,\theta,z,t); \qquad k = (r,z,T); 0 \leq r \leq R_a;\ 0 \leq \theta \leq 2\pi;\ 0 \leq z \leq H;\ t \geq 0$$

Equation: $$\frac{\partial^2 T}{\partial r^2} + \frac{1}{r}\frac{\partial T}{\partial r} + \frac{1}{r^2}\frac{\partial^2 T}{\partial \theta^2} + \frac{\partial^2 T}{\partial z^2} = \alpha \frac{\partial T}{\partial t}$$

B.C.: TOP: $$k_1 \frac{\partial T}{\partial z}(r,\theta,0,t) = \alpha Q_i - h_{CT}(T(r,\theta,0,t) - T_{CT}) - \alpha\sigma\,(T^4(r,\theta,0,t) - T_{CT}^4)$$

SIDE: $$k_1 \frac{\partial T}{\partial r}(R_a,\theta,z,t) = -h_{CR}(T(R_a,\theta,z,t) - T_{CR})$$

BOTTOM:
$$\begin{cases} k_1 \dfrac{\partial T}{\partial z}(r,\theta,H,t) = -h_{CB}\,(T(r,\theta,H,t) - T_{CB}) \ ; \ R_s \leq r \leq R_a \\ k_2 \dfrac{\partial T}{\partial z}(r,\theta,H,t) = -h_{CB}\,(T,r,\theta,H,t) - T_{CB} \ ; \ 0 \leq r \leq R_s \end{cases}$$

CENTER: $$|\,T(0,\theta,z,t)\,| < \infty$$

I.C. $$T(r,\theta,z,0) = T_{CI}\,(r,\theta,z)$$

Figure 2. - General case and formulation.

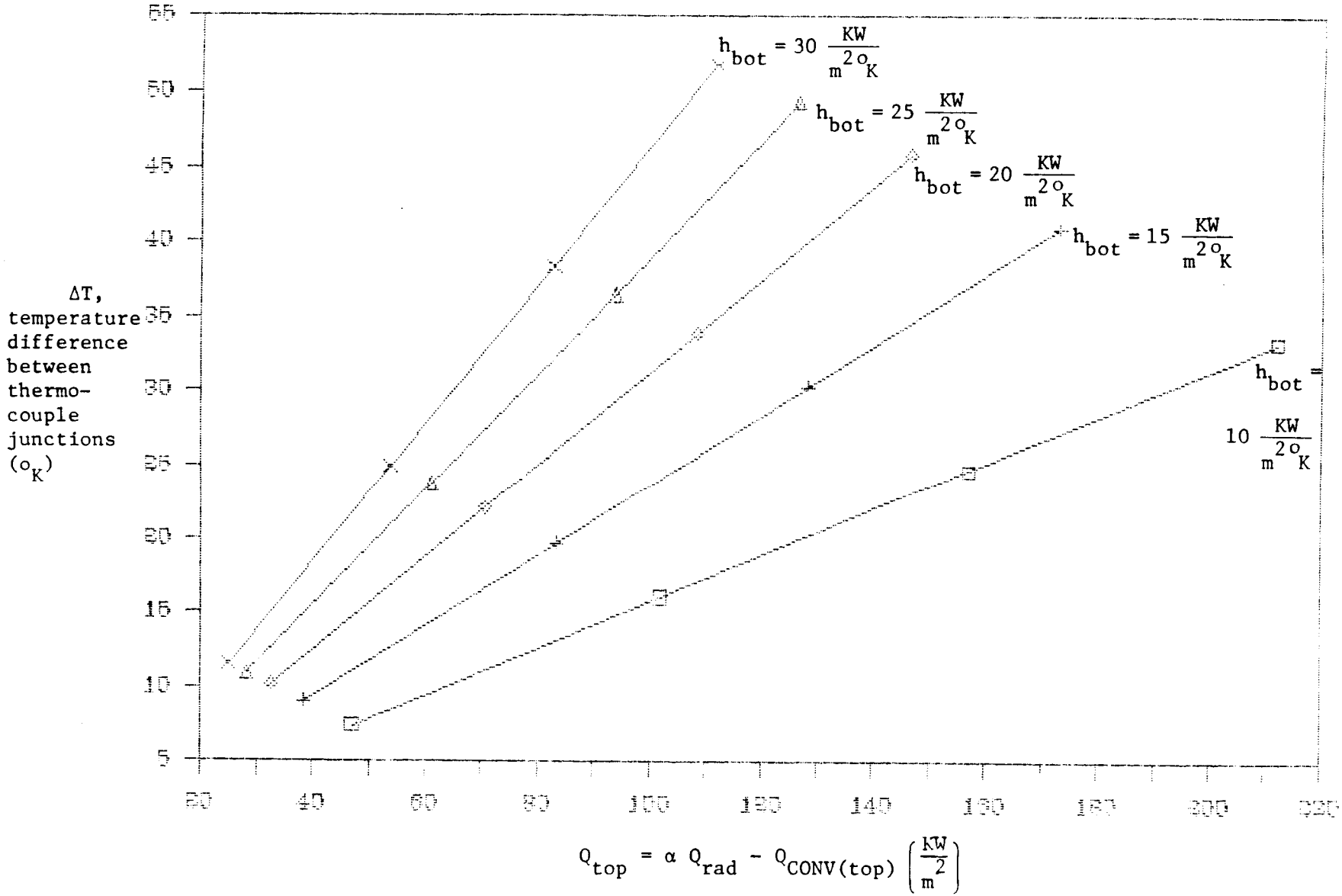

Figure 3. - Calibration curves for several values of h_{bot}. Note that h_{top} = 10 KW/m^2°K is constant and uniform for all cases.

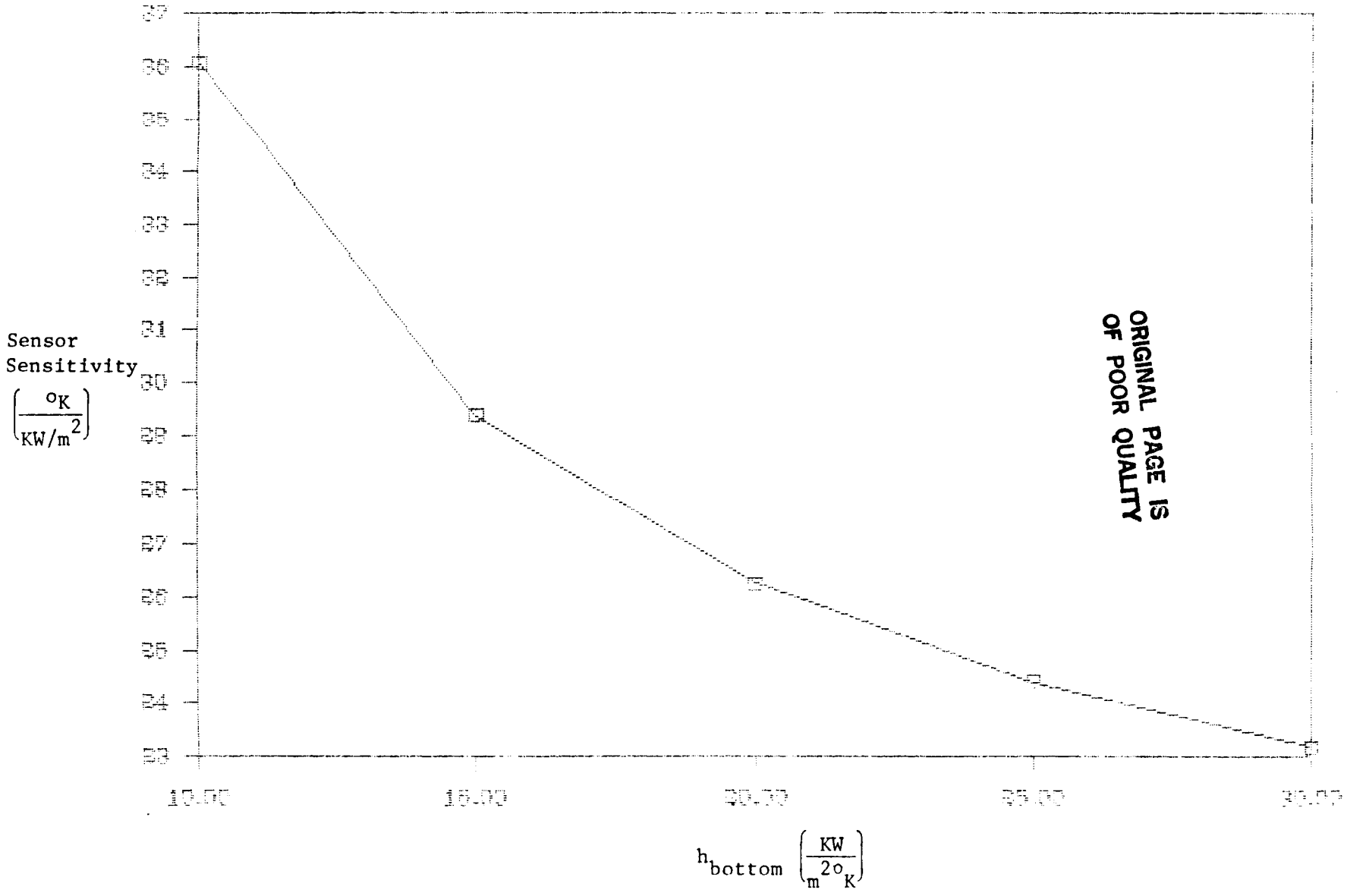

Figure 4. - Variation of sensor sensitivity with h_{bottom}. Note that h_{top} = 10 $KW/m^2 {}^{o}K$ was fixed and uniform in all cases.

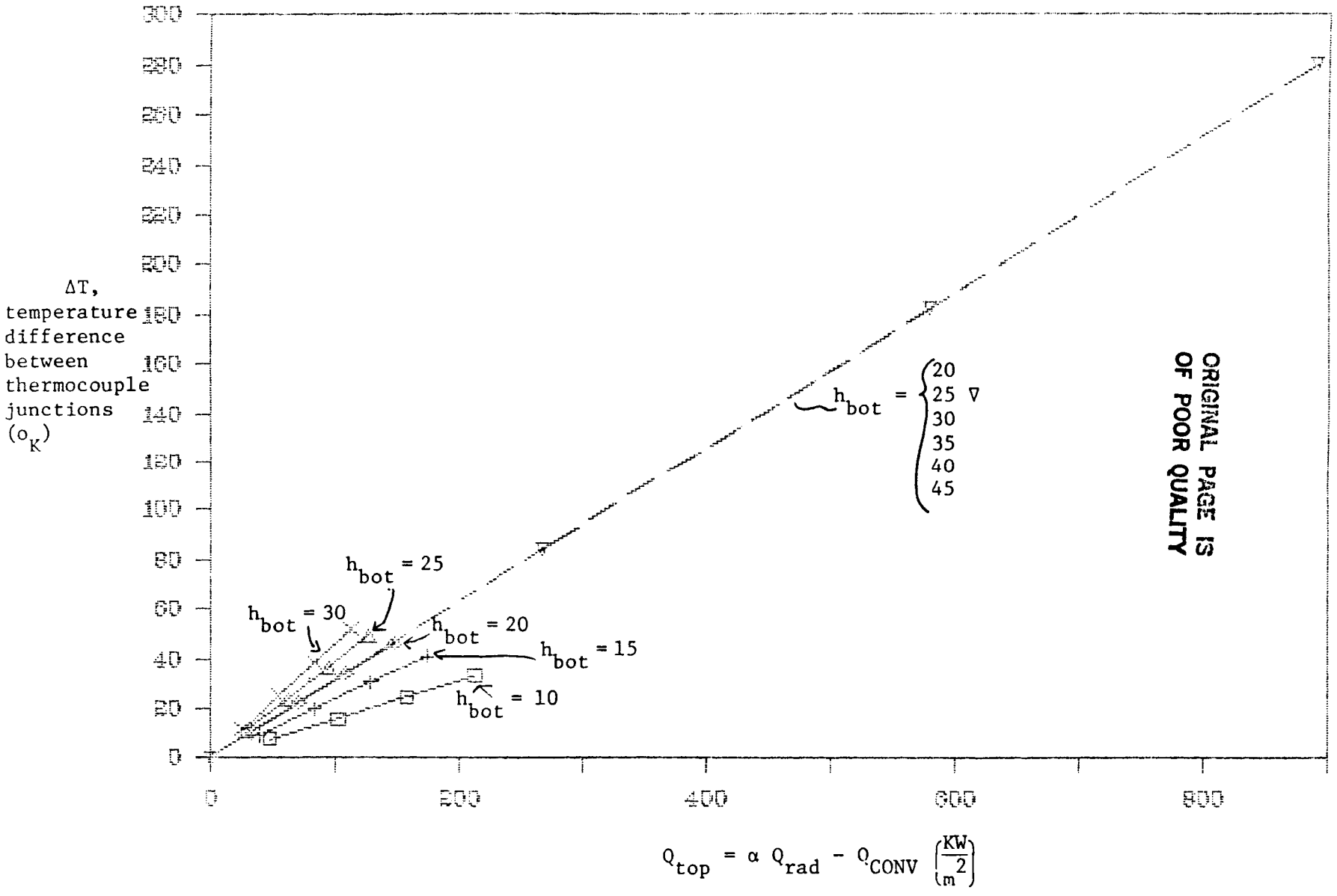

Figure 5. - Comparison of calibration curves for (1) large top-side cooling solid curves (h_{top} = 10 KW/m^2°K) - 5 curves and (2) small top-side cooling broken line (h_{top} = 0 KW/m^2°K) - 5 separate curves all on same line.